JOURNAL OF AIRCRAFT
Vol. 30, No. 6, Nov.–Dec. 1993

Design Tradeoffs on Scramjet Engine Integrated Hypersonic Waverider Vehicles

Mary Kae Lockwood O'Neill* and Mark J. Lewis†
University of Maryland, College Park, Maryland 20742

Two classes of airbreathing hypersonic vehicle concepts, one for primarily cruise missions and the other for accelerator type missions, are presented. Both are designed with waverider airframes and hydrogen-fueled scramjet engine modules. Cruise configurations are optimized for the product of *Isp* and *L/D* while matching lift to weight, corrected for centrifugal force, and thrust to drag at some equivalence ratio. Accelerator configurations are optimized for effective specific impulse while matching lift to weight, corrected for centrifugal force, at an equivalence ratio of 1. The method and computer code developed to optimize the configurations is discussed. The features and design tradeoffs for each class of vehicles are described. Recently available weight estimates for all-body waveriders have had a significant impact on the integrated configurations. A 60-m Mach 8 vehicle, flying at 30.3-km altitude optimized for cruise, has a *L/D* of 4.7 and an *Isp* of 2786 s. A 60-m Mach 14 accelerator, flying at 36.9-km altitude, has an Isp_{eff} of 531 s.

Nomenclature

A = area
D = drag
F_{cent} = centrifugal force
g = gravity
h = altitude
Isp = specific impulse
Isp_{eff} = $(T - D)/(g \times \dot{m}_f)$, effective specific impulse
L = lift
M = Mach number
$\dot{m}_f$ = mass flow rate of fuel
p = pressure
q_{inf} = freestream dynamic pressure
R_{Earth} = radius of Earth
S = reference area
T = thrust, temperature
V = velocity
V = vehicle volume
W = vehicle weight
W_{eff} = effective weight, $W - F_{cent}$
Z_{cp} = axial location of c.p. measured as a percentage of vehicle length from the nose
β = conical shock angle
γ = ratio of specific heats
ρ_v = vehicle density
ϕ = equivalence ratio

Subscripts
cap = engine capture
comb = combustor
p = planform

Introduction

AIRBREATHING hypersonic vehicles, both cruise and accelerators, require highly integrated engine/airframes to reduce total vehicle drag at hypersonic speeds, as well as to reduce total weight. The forebody of the vehicle acts as a precompression surface for the engine, and the aftbody of the vehicle becomes a nozzle, which is the motivation for developing the airframe and engine as one system in this study.

At hypersonic Mach numbers, the centrifugal force on a vehicle is no longer negligible. F_{cent} is

$$F_{cent} = M[V^2/(R_{Earth} + h)]$$

where M = vehicle mass. For a small flight path angle, which is a reasonable assumption for an airbreathing accelerator as well as a cruise vehicle, the centrifugal force acts in the direction of lift. An effective vehicle weight can be defined by $W_{eff} = W - F_{cent}$. As examples of the relative magnitude of the centrifugal force, at Mach 8 $F_{cent}/W = 0.10$, and at Mach 14 $F_{cent}/W = 0.31$.

A successfully integrated engine/airframe accelerator vehicle must yield a high Isp_{eff}.[1] Since the flight path angle will be small, the lift and effective weight of the vehicle should be approximately equal. For a cruise vehicle, an effectively integrated engine/airframe must yield a high $Isp \times (L/D)$ for maximum range as given by the Breguet range equation. Matching thrust and drag at some equivalence ratio less than 1, and matching lift and effective weight is also required. Low trim drag, by balancing the forebody and nozzle forces, is important for both types of vehicles.

There is an inherent tradeoff between producing thrust and lift in an airbreathing hypersonic vehicle since the vehicle and engine are so highly coupled. For example, the angle and area of the nozzle upper wall have a significant effect on the relative magnitudes of the thrust and lift that it produces. Also, since the mass flow entering the engine first passes over a portion of the forebody, a percentage of the lift generated by this part of forebody is negated by turning the airstream into the engine.

The overall performance of both cruise and accelerator vehicles is affected by the uniformity of the flowfield entering the combustor. Uniform mass flux, pressure, and temperature are essential for effective combustion to occur. Since the vehicle forebody determines the properties of the flowfield provided to the engine, this forebody flowfield itself must be uniform, both spanwise and along the height of the inlet.

For effective combustion to occur in a reasonable length combustor, pressures between 25–100 kPa, and temperatures, between 1000–2000 K, must be provided to the com-

Presented as Paper 92-1205 at the AIAA 1st Aerospace Design Conference, Irvine, CA, Feb. 1992; received Feb. 28, 1992; revision received July 10, 1992; accepted for publication Oct. 30, 1992.

*Minta-Martin Fellow, Department of Aerospace Engineering. Student Member AIAA.

†Assistant Professor, Department of Aerospace Engineering. Member AIAA.

bustor entrance. Properties outside these ranges would result in either excessive ignition times or excessive reaction times, thereby requiring impractical combustor lengths.[2,3] In combination with inlet design, flight altitude plays a dominant role in establishing the thermodynamic properties at the combustor entrance. To maintain the entrance temperature and pressure within the ranges discussed, there is an altitude ceiling and floor. The altitude ceiling corresponds to the maximum allowable combustor entrance temperature of 2000 K and the minimum allowable entrance pressure of 25 kPa.[2]

Waverider airframes have been shown to be promising configurations for hypersonic vehicles. They have been shown both computationally[4,5] and experimentally[6] to yield higher L/D ratios at their design point than other hypersonic airframe configurations, which is particularly important for cruise vehicles. In addition, the waverider's L/D has been shown computationally to remain high at off-design hypersonic Mach numbers.[7] Waveriders have also been designed with rounded leading edges to sufficiently reduce heat transfer.[8] Results show that rounding the leading edges causes only a small decrease in L/D, on the order of 5% for a 60-m vehicle. Waveriders have also been shown to be promising configurations for scramjet integration.[9] Waveriders can be designed to provide uniform flowfields to the engine inlet, and the contained flowfield on the undersurface of the waverider yields no crossflow. Also, flying at off-design hypersonic Mach numbers, waveriders with rounded leading edges have been shown computationally to maintain fairly uniform flowfields at the engine inlet plane.[7] Another feature of the waverider that makes it effective for engine integration is the inverse method by which it's designed. It allows the waverider to be developed to provide the engine with the required flowfield properties.

The code developed for this study generates conically derived waveriders specifically for scramjet integration. The combustor is modeled with quasi-one-dimensional flow and the inlet and nozzle are modeled with two-dimensional planar flow. Aerodynamic forces on an integrated configuration can be determined relatively quickly, yielding reasonable computation times for optimization. Configurations in this study are optimized for the product of Isp and L/D for cruise, or Isp_{eff} for an accelerator. The results of an optimization include the forebody shape, inlet shape, engine location along the length of the vehicle, engine span, vehicle volume, and the approximate values for effective specific impulse, L/D, specific impulse, and c.p. for the optimized configuration.[10]

Engine/Airframe Integration Model

Waverider

Waveriders are developed for scramjet integration on accelerator vehicles as follows: For an accelerator it is important to maximize engine mass capture by utilizing essentially the entire airstream between the undersurface of the vehicle and the bow shock as mass flow into the inlet. It is also desirable to use many identical scramjet modules spanwise across the undersurface of the vehicle. This allows the development of a single module, thus reducing development cost. For an axisymmetric-generated waverider, the shape of the bow shock in the engine inlet plane, as shown in Fig. 1, is circular. Therefore, to maximize mass capture, the cowl lip should be a circular arc and as close to the bow shock as possible. To have uniform inlet height for identical engine modules, the shape of the vehicle undersurface, or inlet curve, at the inlet station should be as circular as possible. In other words, the desired general shape of the waverider at the inlet station is known. Waveriders in this study are therefore traced starting from the scramjet inlet station. The forebody undersurface is formed by streamlines traced forward from the known inlet curve to the bow shock. The upper surface is formed by freestream streamlines traced rearward from the undersurface streamline/shock intersection.

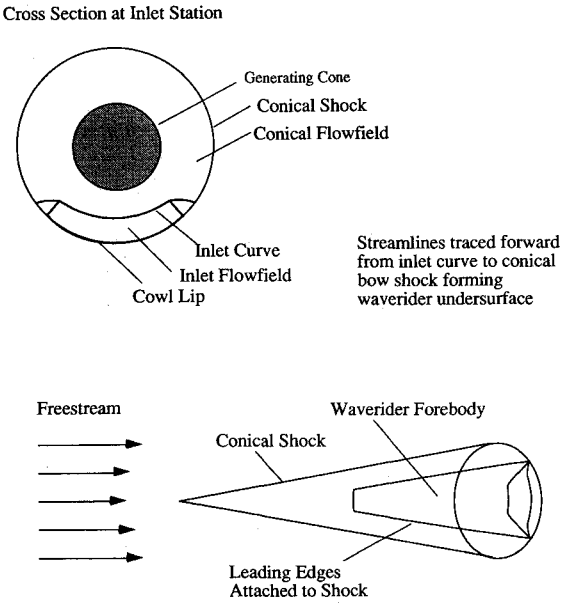

Fig. 1 Waverider forebody construction from circular arc inlet curve.

Waveriders generated from circular arc inlet curves have a cusped leading edge at the nose and concave upper surfaces.[2] From heat transfer and volume efficiency considerations, these vehicles are probably not practical. Therefore, the requirement for inlet height uniformity with span is relaxed somewhat and the inlet curve is allowed to be elliptic instead of circular. This small compromise in inlet height uniformity leads to a substantial change in the forebody shape.

The engine span for a cruise vehicle, as shown in the results below, is a much smaller percentage of the vehicle span at the inlet station than for an accelerator. Also maximizing mass flow by matching the cowl to the shock for a cruise configuration is not as critical, since the primary objective is cruise range instead of acceleration. Therefore, there is more flexibility in the shape of the inlet curve for a cruise vehicle in terms of integrating it with a scramjet. However, it is still important to maintain uniform flow both along the height of one module and from module to module. Also, a smooth vehicle undersurface where the engines are to be installed is desirable. Therefore, waveriders are generated in a similar fashion for both cruise vehicles and accelerators. The primary difference is that the radius of the cowl lip in the inlet plane of the cruise vehicle is allowed to be less than the bow shock radius, and the elliptic section of the inlet curve for a cruise vehicle is allowed to be more highly elliptic than for an accelerator.

Inlet curves used in this study are comprised of a section of an ellipse, which is centered at the generating shock circle, and a wing curve that connects the elliptic section to the circular shock at the tail station as shown in Fig. 2. The wing curve is developed from a spline of three points at the outboard-most section of the ellipse, and four additional points located at the trailing edge of the vehicle. Note that the outboard-most point is required to lie on the shock. Ten parameters therefore govern the shape of the inlet curve in this study: 1) semiminor ellipse axis, 2) semimajor ellipse axis, 3) span of the ellipse, 4–9) the x and y coordinates of three points, and 10) the y coordinate of the outboard-most point.

One of the results of the optimization, in addition to the shape of the forebody, is the length of the forebody relative to the vehicle length. This is determined by the location of the inlet curve relative to the shock. The farther the inlet curve is from the shock, the longer the forebody for a fixed-length vehicle.

The inlet station in the generating flowfield, which is also the axial location of the cowl lip, is allowed to vary in the

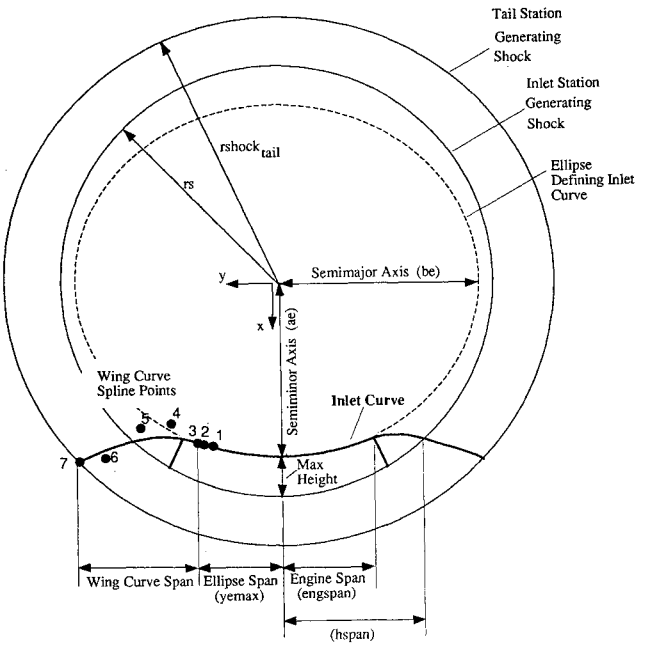

Fig. 2 Optimization parameters in the cross section of the generating flow.

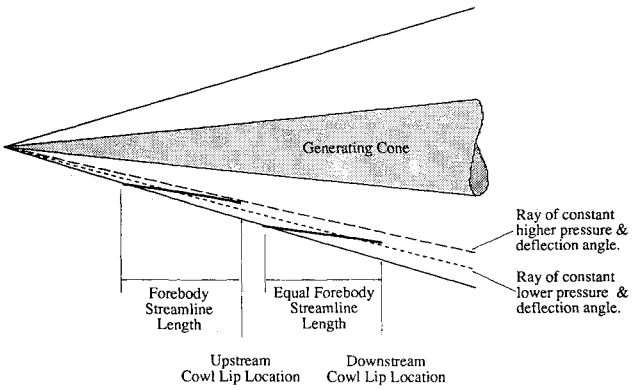

Fig. 3 Cowl lip axial location in generating conical flowfield.

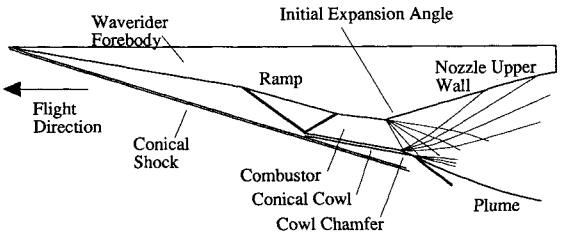

Fig. 4 Inlet ramp and nozzle configuration.

optimization. As illustrated in Fig. 3, the cowl lip location affects the pressure and the angle of the undersurface of the vehicle, due to the nature of the conical flowfield. Therefore, vehicle lift and drag are affected. Locating the cowl lip farther downstream in the generating flow decreases the pressure on a forebody streamline of the same length, and also decreases its angle to the freestream. Note also that for a given inlet height, the vertical gradients in flowfield properties along that height decrease as the cowl lip location moves farther downstream. The cowl lip location also dictates the maximum cowl lip radius in the cross-sectional plane.

Previous waverider optimization studies[4,5,8,11] that have generated waveriders from leading-edge curves, have changed the axial location of the waverider in the generating flowfield by scaling the waverider. In other words, given a leading-edge curve and a generating flowfield, a waverider of some length

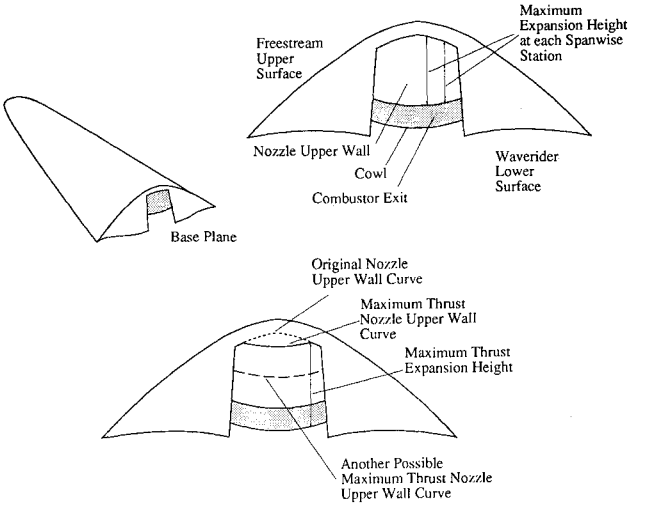

Fig. 5 Design of nozzle upper wall surface. Top: each upper wall contour expanded to maximum available height. Bottom: maximum thrust expansion height.

results. If the length is less than the desired vehicle length, the waverider is scaled up. This effectively moves the waverider farther aft in the generating flowfield.

The generating conical shock angle, which is also a design variable in the optimization, also has an effect on the pressure and lower surface deflection angle. In addition, it affects the relative amount of compression produced by the forebody compared to that produced by the scramjet inlet ramp to yield the required combustor entrance conditions.

Inlet, Cowl, and Nozzle

The inlet and nozzle designs chosen for this study are shown in Fig. 4. The inlet flow is approximated as two-dimensional planar with $\gamma = 1.4$, where mass-averaged values of the thermodynamic variables, Mach number, and flow angle are determined from the known properties at the waverider forebody inlet station. Ramp shock and reflected shock strengths are governed by the given combustor entrance temperature. The flight altitude is determined by the combustor pressure.

The cowl is traced from the conical flowfield. For an accelerator vehicle the cowl lip radius is set equal to that of the bow shock, shown in Fig. 4. For a cruise vehicle, the cowl lip radius is one of the variables in the optimization.

The flowfield through the nozzle is assumed to be frozen at the composition exiting the combustor. The nozzle is then designed for isentropic flow using the two-dimensional planar method of characteristics as shown in Fig. 4. In this study, one of the variables in the optimization is the distance the cowl extends into the nozzle flowfield. The minimum distance, as shown in Fig. 4, is such that the cowl chamfer intersects the first characteristic emanating from the upper wall.[12]

The nozzle contour is determined at several spanwise locations at the combustor exit. The contours are determined such that nozzle thrust is maximized in the direction of flight for a given nozzle box size. The box size is governed by the location of the vehicle upper surface, the combustor exit span and its distance from the vehicle upper surface, the cowl length, and finally, the nozzle length which is the remaining vehicle length after the forebody, inlet, and combustor lengths for the current vehicle have been determined. Limits are set on the inlet curve location to ensure reasonable ratios of forebody to nozzle length. Figure 5 shows the maximum nozzle expansion if each nozzle contour were to expand to the vehicle upper surface with some clearance, and a couple possible maximum thrust expansion surfaces. This analysis is reasonable, provided that characteristics reflected from the nozzle plume do not intersect the nozzle upper wall, and that the three-dimensional effects in the nozzle are second-order.

Scramjet/Combustor

Quasi-one-dimensional equations, based on those in Ref. 13, which include area variation, heat addition, friction, mass injection, variation in molecular weight, and ratio of specific heats, are used to analyze the flowfield through the combustor of one engine module. The area variation is designed to provide constant pressure combustion. The equations are solved step by step from the combustor entrance to exit using a fourth-order Runge-Kutta technique.

The rate of combustion, and therefore, the combustor length, is dependent on both the rate of mixing, ignition, and reaction. Ignition and reaction times are determined from Rogers and Schexnayder,[14] based on the combustor pressure and entrance temperature. The mixing rate is based on a mixing efficiency[15] derived from experimental results of cold flow mixing with perpendicular injection.[16,17] The total heat released is based on complete combustion from the initial conditions.[18]

For the set of optimized vehicles presented in this article, an equivalence ratio of 1 is used for the accelerator vehicles and 0.9 for the cruise vehicles. The equivalence ratio for cruise vehicles is chosen somewhat arbitrarily. It must be less than 1 when matching thrust and drag, or the desired cruise Mach number would not be reached. Also, some margin during cruise is desired. However, making the equivalence ratio too small will either force the engine span to become excessively large, or at the extreme, not produce enough thrust to overcome drag. Combustor lengths for vehicles in this study vary from 1.4 to 2.6 m for complete combustion at flight Mach numbers from 8 to 14, respectively.

Base Area Reduction

Waveriders designed for cruise often have much larger base areas, as compared to accelerator vehicles, since engine spans are smaller, and therefore, nozzles take up a much smaller percentage of the tail span. Reducing the base drag for flight through subsonic, transonic, and supersonic regimes is important. Therefore, for the cruise vehicles, the upper surface of the vehicle is expanded to decrease the base areas. The top left view in Fig. 6 shows the large base area of a cruise vehicle optimized without expansion, and Fig. 7 shows the reduced base area with upper surface expansion. Note in Fig.

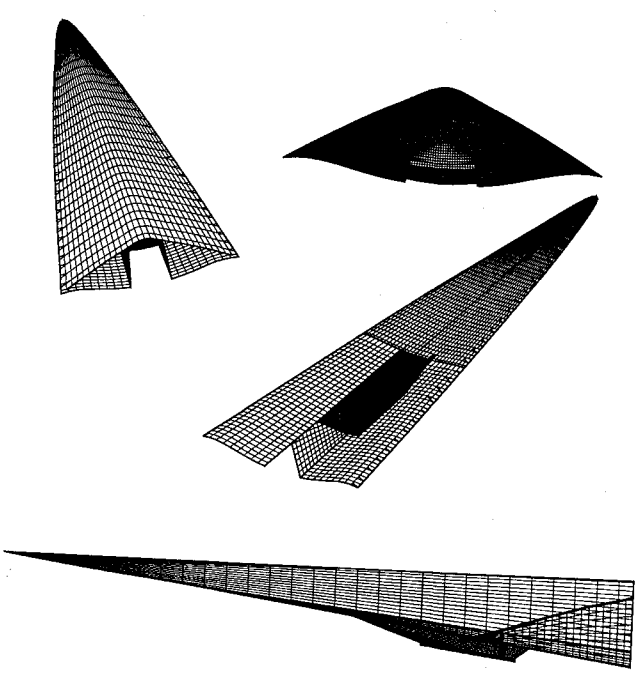

Fig. 6 Mach 10 cruise vehicle without upper surface expansion and $L \neq W_{\text{eff}}$.

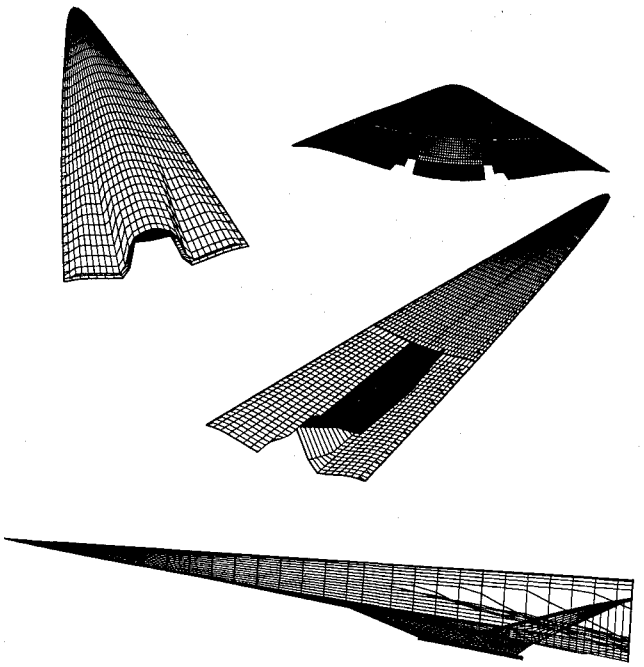

Fig. 7 Mach 10 cruise vehicle with $L \neq W_{\text{eff}}$. $\beta_{\min} = 11$ deg, $p_{\text{comb}} = 50$ kPa, $T_{\text{comb}} = 1000$ K, $L/W_{\text{eff}} = 0.91$.

7 that the nozzle side wall is smoothed into the outboard surface on the compression side of the vehicle, and the upper surface tail curve is matched to the lower surface curve at the tail. Unit square curves developed by Sobieczky[19] were used for this purpose. A maximum expansion angle of 12 deg, considered to be a design maximum for reducing drag by Raymer,[20] was then used to expand the upper surface from freestream flow to the prescribed tail curve. The configurations in Figs. 6 and 7 are discussed further in the results.

Force Calculation

The values of L/D, Isp, and Isp_{eff} for a highly integrated vehicle are dependent, in part, on how the forces are accounted for. In this work, all vertical forces, including those generated by the propulsion system, and the vertical component of engine momentum are added for lift. To calculate the drag, all viscous drag forces are included, but only the drag direction pressure forces are included. Exceptions to this include the base drag force which assumes freestream pressure acting on the base area, the forward pressure force on the inside entrance surface of the cowl, and the forward pressure force on the vehicle upper surface when it has been expanded. These are all added into the total drag. The control volume used for the force calculation is shown in Fig. 8.

Weight is determined from the known vehicle volume calculated by the code and an overall vehicle density based on results from Ardema et al.[21] for a Mach 6 all-body waverider vehicle with hydrogen fuel. The total vehicle density, gross takeoff weight divided by the total vehicle volume, for the all-body waverider, was 124.2 kg/m^3.[21] The vehicle was 63.7 m in length and had a 1463.5-m^3 volume. For the present study, the Mach 8–10 vehicles were calculated with vehicle densities 10% greater than the Mach 6 all-body waverider vehicle. The vehicle density used was 15% greater for the Mach 12 vehicle and 20% greater for the Mach 14 vehicle. Studies have not been completed on all-body waverider weights for these Mach numbers, so these values are approximations. The higher densities were used to account for the potentially higher engine and cooling system weights for higher Mach number vehicles. The effective vehicle weight is calculated by subtracting the centrifugal force described in the introduction from the vehicle weight calculated here, using the vehicle

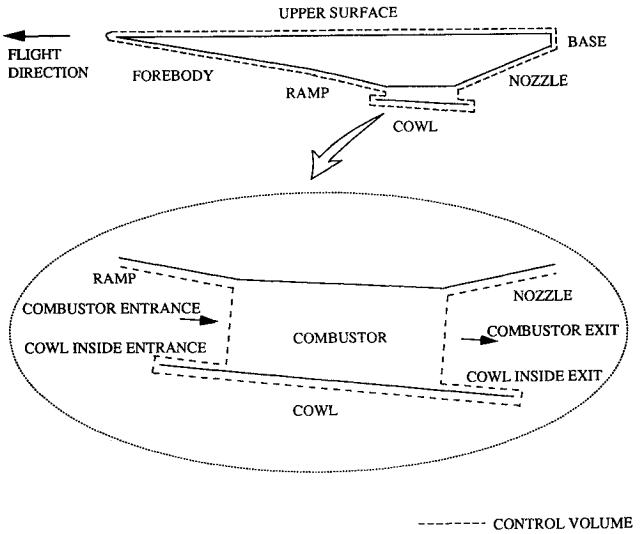

Fig. 8 Control volume for force calculation.

density and volume. To determine the effect that the estimated density has on the configuration, a Mach 10 cruise vehicle and a Mach 14 accelerator were optimized without matching lift to effective weight, as discussed in the results.

Objective Functions

The waverider/scramjet configuration is optimized for $Isp \times (L/D)$ with $L = W_{\text{eff}}$, $T = D$, and $\phi = 0.9$ to maximize cruise range at the design point. Therefore, the objective function F_1 to be minimized for a cruise configuration is

$$F_1 = (L/W_{\text{eff}})^a (T/D)^b (D/L \times Isp)$$

$$L > W_{\text{eff}} \quad a > 1, \qquad L < W_{\text{eff}} \quad a < -1$$

$$T > D \quad b > 1, \qquad D < T \quad b < -1$$

The magnitudes of a and b in the above objective functions are greater than 1 to maintain a large enough penalty on the objective functions as the L/W_{eff} and T/D approach 1. Typical values are $a = 5$ and $b = 4$. It is also important to note that their signs change depending upon the relative magnitudes of lift and effective weight or thrust and drag. The flight altitude, which is set by the specified combustor entrance conditions, also has a considerable effect on matching lift and effective weight. For example, if the altitude is too high, it is possible that there will not be a solution which produces enough lift to equal the effective weight.

For an accelerator, the configuration was optimized for Isp_{eff} with $L = W_{\text{eff}}$ at the design point. One of the next steps for future work would be to optimize the accelerator configuration together with the flight path. However, achieving a positive value for thrust minus drag (or positive Isp_{eff}) for an airbreathing vehicle at the higher hypersonic Mach numbers is one of the critical design points. Therefore, optimizing for maximum Isp_{eff} at the highest Mach number of scramjet operation for a given vehicle is a good first step. The objective function F_2 to be minimized for an accelerator is therefore

$$F_2 = (L/W)^a (1/Isp_{\text{eff}})$$

$$L > W_{\text{eff}} \quad a > 1, \qquad L < W_{\text{eff}} \quad a < -1$$

At higher Mach numbers in particular, the effective specific impulse is negative for some designs. If a design has a negative Isp_{eff}, a penalty is assigned to the objective function.

Optimization Parameters and Design Variables

The parameters that remain fixed throughout an optimization are flight Mach number, combustor entrance pressure and temperature, combustor equivalence ratio, vehicle length, vehicle density, and vehicle wall temperature.

Fourteen design variables are allowed to vary in the optimization for an accelerator and fifteen for a cruise vehicle. Ten describe the inlet curve shape as detailed in the waverider section. Two describe the size of the engine box: 1) the percentage of vehicle spanned by engine at the inlet station, and 2) the length the cowl extends into the nozzle flowfield. The generating or bow shock angle β, and the cowl lip axial location on the generating shock, are also design variables in the optimization. For a cruise vehicle only, the radius of the cowl as a percentage of the bow shock radius at the inlet station is a design variable. These 14 or 15 variables, along with the parameters that are fixed at the start of the optimization, define the entire integrated configuration and therefore yield the value of the objective function for that configuration.

Side constraints are placed on the design variables and include the minimum and maximum values for forebody length as a percentage of total vehicle length, the ellipticity of the inlet curve which is allowed to be greater for the cruise vehicles, the minimum and maximum values for the engine span and cowl length, the engine height uniformity, and the minimum and maximum values of the cowl radius for the cruise vehicle. Side constraints are also placed on the generating shock angles β, such that $\beta_{\min} \leq \beta \leq 18$ deg, where $\beta_{\min} \geq 10$ deg, depending on the optimization run. For the Mach number range considered in this study, generating shock angles greater than 18 deg yield low values of L/D and Isp_{eff}, and angles less than 10 deg result in vehicles with small volume. As described in the results, $\beta_{\min}$ is the most important and most often active side constraint at the optimum.

Behavior constraints are also imposed and include the requirement that the radius of the inlet curve increases with distance in the spanwise direction, and that the vehicle tail does not hit the ground when the vehicle is pitched up for takeoff.[20] Using $(L/W_{\text{eff}})^a$ and $(T/D)^b$ in the objective function to drive the design toward $L = W_{\text{eff}}$ and $T = D$ could also be considered behavior constraints which are placed in the objective function. By including the constraints in the objective function, the shape of the design space itself is altered. Designs have been optimized, as will be discussed in the results, with and without imposing a penalty on the objective function for a ratio of $L/W_{\text{eff}} \neq 1$. In some cases the optimized vehicle configuration and characteristics are similar with and without the penalty. In other cases there is a significant difference between the two optimized vehicles. Finally, there are cases when the optimizer cannot produce a vehicle with $L/W_{\text{eff}} = 1$. The results are dependent on the flight altitude, which is determined by the combustor entrance conditions, and the range of generating shock angles β for a given optimization.

The zero-order nonlinear simplex method by Nelder and Mead[22] was used to optimize the system. This optimization technique has been used successfully in previous waverider work.[4,5,8,9,11] Convergence usually occurs within approximately 80 iterations.

Results

Hypersonic Cruise Vehicle

Conically-derived waveriders integrated with scramjet engines were optimized at flight Mach numbers of 8–10 with the objective function for cruise as given in the optimization section. All configurations discussed in this document are 60 m in length and were run with an equivalence ratio of 0.9. All resulting cruise altitudes range between 30–33 km.

Baseline cruise vehicles were run at combustor entrance conditions to yield dynamic pressures of approximately 50 kPa. The curve labeled "baseline cruise" in Fig. 9 shows the variation of L/D with Mach number for these configurations. The decrease in L/D with Mach number is caused primarily

by the increased engine size required to match thrust to drag at the higher Mach numbers. Lift produced by the combination of the ramp, cowl, and nozzle of the engine is close to zero. The engine drag, primarily from the ramp, is large, however. Therefore, the engine increases the vehicle drag without producing much lift.

Table 1 shows the parameters maintained fixed throughout an optimization and the resulting characteristics of the optimized baseline configurations. Perspective and side views of the Mach 8 and 10 baseline configurations are shown in Figs. 10 and 11. Note the reduction in base area achieved by the upper surface expansion in all vehicles. There appears to be a channel on each side of the engine when viewed from the base. This is actually the region where the compression surface of the vehicle is blended into the nozzle, as shown in the perspective views of the lower surface of the vehicle. The sharpness of the curve is partly due to the resolution of the graphics.

As Mach number increases, the vehicle planform shape becomes more pointed, and the upper surface-cross sectional shape changes from flat for the Mach 8 configuration to more pointed for the Mach 10 vehicle. These characteristics result from the more elliptic-shaped inlet curves which result with increasing Mach number. Also engine size increases with increasing Mach number. Note from the base view of the Mach 10 vehicle in Fig. 11 that the nozzle expansion height, which maximizes thrust as shown, is less than the geometric expansion height available.

Figures 12 and 13 show the lift and drag distributions on the Mach 10 cruise vehicle. The bar labeled "forebody" includes the undersurface forward of the ramp and the complete upper surface. "Outboard" refers to the section of the undersurface outboard of the engine and downstream from the start of the ramp. "Ramp" represents the force on the entire ramp, including the section that extends past the cowl lip to the entrance of the combustor. "Cowl exterior" includes the outside lower and side surfaces of the cowl. "Cowl entrance" is the inside surface of the cowl upstream of the combustor and "cowl exit" is the inside surface downstream of the combustor. Recall that the cowl entrance force is added into the drag. "Nozzle" includes the upper wall and side walls of the nozzle. "Engine" is the momentum change through the combustor. "Total" is the sum of all of the lift or thrust and drag forces.

Note from Fig. 12 that the sum of the ramp, cowl, and nozzle lift is approximately zero. Note from Fig. 13 that the ramp adds an additional 50% in drag to the vehicle. The trend is similar for the lower Mach number vehicles, thus illustrating that increasing engine size does reduce the overall vehicle L/D as stated previously.

To remove the effect of the estimated density on the configuration, a Mach 10 configuration was run without penalizing the objective function for having lift unequal to effective weight. In other words, the ratio $(L/W_{\text{eff}})^a$ was removed from the objective function. This $L \neq W_{\text{eff}}$ configuration was run at the same conditions as the Mach 10 baseline configuration, including the value of the minimum generating shock angle, $\beta_{\min} = 11$ deg. The resulting configuration is shown in Fig.

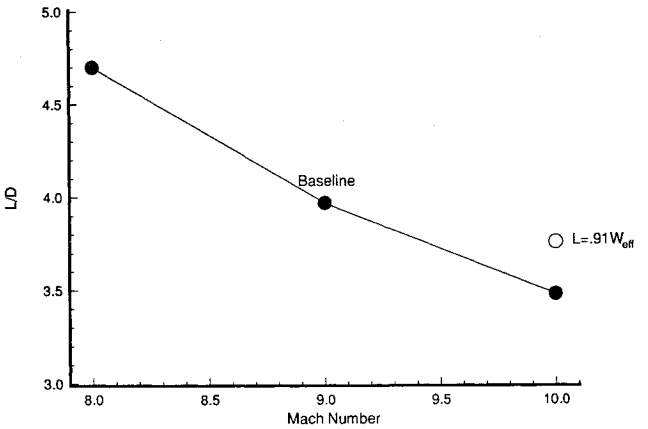

Fig. 9 Variation of lift-to-drag ratio with Mach number for cruise.

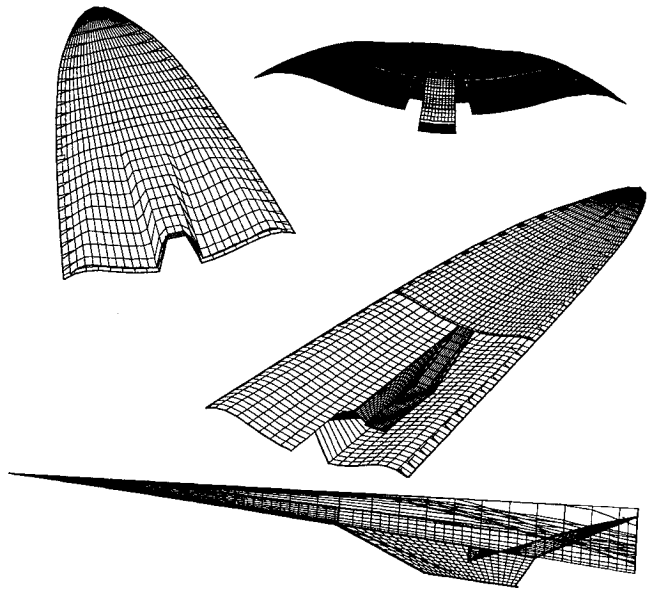

Fig. 10 Mach 8 baseline cruise scramjet integrated waverider. $\beta_{\min}$ = 10 deg, p_{comb} = 75 kPa, T_{comb} = 1000 K. Top left: top view of vehicle. Top right: view from tail. Center: undersurface with engine ramp, cowl and nozzle. Bottom: side view.

Table 1 Cruise configuration results

Parameters	Baseline			$L \neq W_{\text{eff}}$	No expansion
Mach number	8	9	10	10	10
ρ_v, kg/m^3	137	137	137	137	137
p_{comb}, kPa	75	62.5	50	50	62.5
T_{comb}, K	1000	1000	1000	1000	1000
Altitude, km	30.3	31.9	33.1	33.1	31.9
q_{inf}, kPa	50.4	51.2	53.3	52.6	63.2
β, deg	10.82	11.42	12.23	11.05	11.17
Volume, m^3	2238	2730	2686	1988	2315
$V^{2/3}/S_p$	0.13	0.14	0.18	0.17	0.19
A_{cap}/S_p	0.015	0.023	0.038	0.025	0.025
Contraction	13.5	14.8	14.6	14.8	15.2
L/W_{eff}	1	1	1	0.91	0.89
L/D	4.70	3.97	3.48	3.76	3.53
Isp, s	2786	2716	2417	2695	2740
Z_{cp}, %	64	62	62	64	62

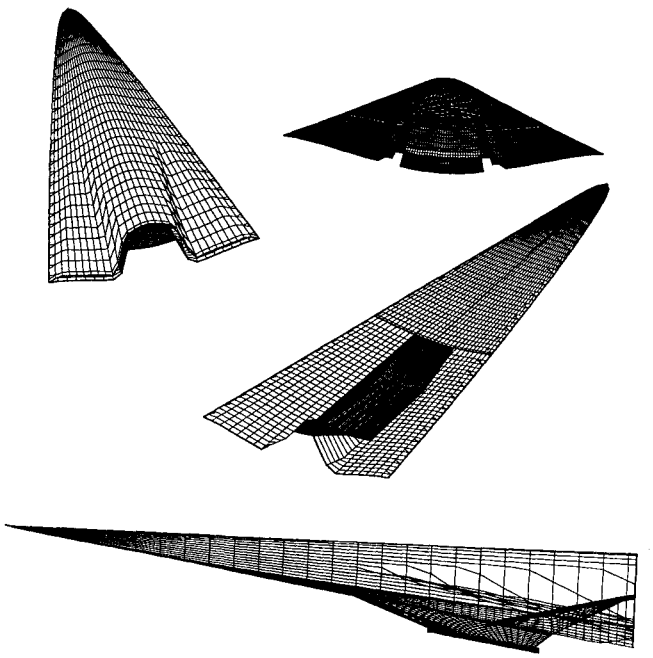

Fig. 11 Mach 10 baseline cruise scramjet integrated waverider. β_{min} = 11 deg, p_{comb} = 50 kPa, T_{comb} = 1000 K.

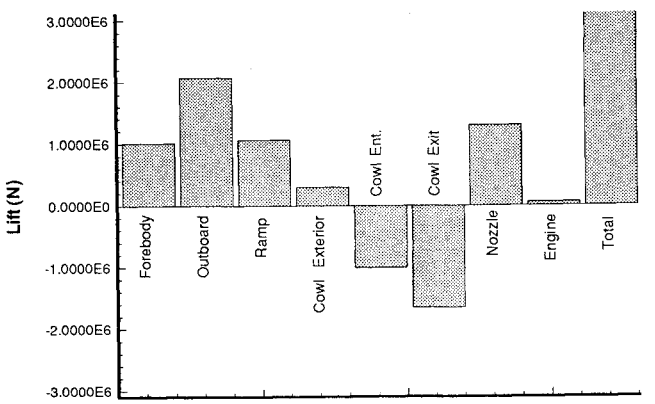

Fig. 12 Lift distribution on Mach 10 baseline cruise vehicle. β_{min} = 11 deg, p_{comb} = 50 kPa, T_{comb} = 1000 K.

7, and the vehicle characteristics are listed in Table 1. Note that the resulting flight altitude and dynamic pressure are approximately the same for both the $L \neq W_{eff}$ configuration and the baseline configuration. However, instead of having $L/W_{eff} = 1$ with $\beta = 12.2$ deg, and $L/D = 3.48$, as for the baseline vehicle, the $L \neq W_{eff}$ configuration has $L/W_{eff} = 0.91$ with $\beta = 11.05$ deg, and $L/D = 3.76$. Thus, to maximize L/D without any consideration for matching lift to effective weight, the optimizer decreased the generating shock angle β to the minimum, β_{min}, which results in a higher value of L/D. To realize this value of L/D, the vehicle would have to be flown at a lower altitude where $L/W_{eff} = 1$. The Mach 10 baseline vehicle is thus optimized and flying at an altitude higher than that which would yield the maximum L/D. To increase the vehicle lift to achieve $L/W_{eff} = 1$ at this altitude, the optimizer increased the generating shock angle to $\beta = 12.2$ deg for the Mach 10 baseline vehicle. Therefore, the mechanism by which the cruise vehicle increases lift to match effective weight is to increase the generating shock angle. The penalty for increasing β to achieve $L = W_{eff}$ for the baseline Mach 10 vehicle is a 7.4% decrease in L/D and a 52% increase in A_{cap}/S_p. The vehicle volume does increase for the baseline configuration as compared to the $L \neq W_{eff}$ configuration by 35%.

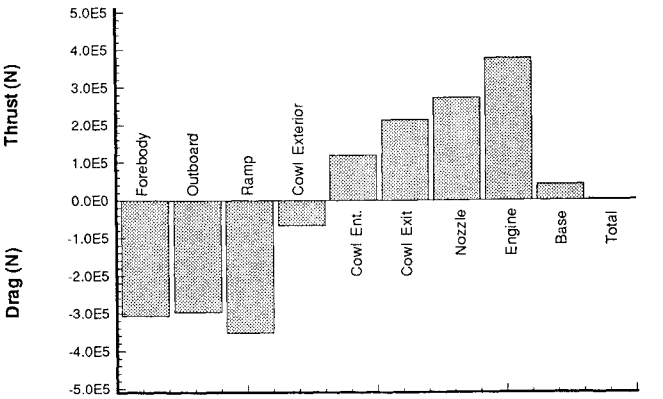

Fig. 13 Drag/thrust distribution on Mach 10 baseline cruise vehicle. β_{min} = 11 deg, p_{comb} = 50 kPa, T_{comb} = 1000 K.

To determine the effect of expanding the upper surface to reduce base drag, a Mach 10 cruise vehicle was optimized without expanding the upper surface. For this case, $\beta_{min} = 11$ deg, $L \neq W_{eff}$, and the combustor entrance conditions are 0.625-atm pressure and 1000 K temperature. The resulting configuration is shown in Fig. 6 and the vehicle characteristics are listed in Table 1. The configuration resulted in $L/W_{eff} = 0.89$ at an altitude of 31.9 km. Thus, the vehicle would yield $L = W_{eff}$ and the maximum value of L/D at a lower altitude. The expanded configuration discussed above, shown in Fig. 7, optimized with $L \neq W_{eff}$, resulted in $L/W_{eff} = 0.91$ at an altitude of 33.1 km. Thus, the altitude to achieve $L = W_{eff}$ for the maximum L/D unexpanded configuration is lower than that for the maximum L/D expanded configuration. This results for two reasons: 1) the unexpanded configuration has a greater volumetric efficiency, and 2) the expansion surface on an expanded configuration increases the vehicle lift. For the unexpanded configuration, $L/D = 3.53$, which is slightly less than that for the expanded configuration. The value of L/D is slightly favored, however, for the unexpanded configuration since freestream pressure is assumed to act on the base, whereas the pressure on the area of the upper surface projected on the base plane is less than the freestream pressure for the expanded configuration. For the unexpanded $L \neq W_{eff}$ configuration, $\beta = 11.17$ deg, demonstrating again that the highest values of L/D correspond to values of β close to the minimum. The volume is greater for the unexpanded configuration as compared to the expanded configuration as shown in Table 1. The two configurations have identical ratios of A_{cap}/S_p.

Hypersonic Accelerator Vehicle

Integrated configurations were optimized with the objective function for an accelerator-type vehicle at Mach 10, 12, and 14. All vehicles are 60 m in length and optimized with $\phi = 1$ and $\beta_{min} = 11$ deg. The baseline configurations are all optimized with combustor entrance conditions to yield dynamic pressures of approximately 60 kPa. Table 2 contains the resulting characteristics for the baseline configurations.

Figure 14 shows the resulting perspective and side views for the Mach 10 accelerator. For the Mach 10 configuration, $Isp_{eff} = 1312$ s, volume = 4135 m^3, and $\beta = 11.40$ deg. Compared to the Mach 10 cruise vehicle shown in Fig. 11, the accelerator has a significantly larger engine span and vehicle volume than the cruise vehicle. Comparing the side views for the two configurations, the engine is significantly farther forward for the accelerator, substantially increasing the nozzle length, as compared to the cruise vehicle. In addition, as shown in the base view, the maximum thrust nozzle is that which expands to the maximum available expansion height. Base area has not been reduced by upper surface expansion for the accelerators. However, the base area is small since the engine span is a large percentage of the vehicle span.

Table 2 Accelerator configuration results

Parameters	Baseline		
Mach number	10	12	14
ρ_v, kg/m^3	137	143	149
p_{comb}, kPa	62.5	75	50
T_{comb}, K	1000	1400	1400
Altitude, km	31.8	34.7	36.9
q_{inf}, kPa	63.5	60.6	61.8
β, deg	11.40	11.97	11.16
Volume, m^3	4135	3258	3902
$V^{2/3}/S_p$	0.15	0.17	0.15
A_{cap}/S_p	0.091	0.080	0.077
Contraction	15.1	20.2	19.0
Isp_{eff}, s	1312	914	531
Isp, s	2356	2484	2039
L/D	2.56	2.40	2.61
Z_{cp}, %	68	67	62

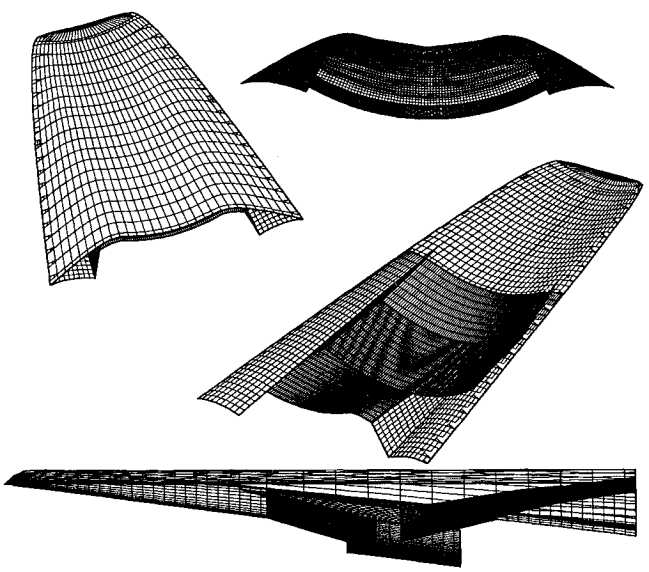

Fig. 14 Mach 10 baseline accelerator. β_{min} = 11 deg, p_{comb} = 62.5 kPa, T_{comb} = 1000 K.

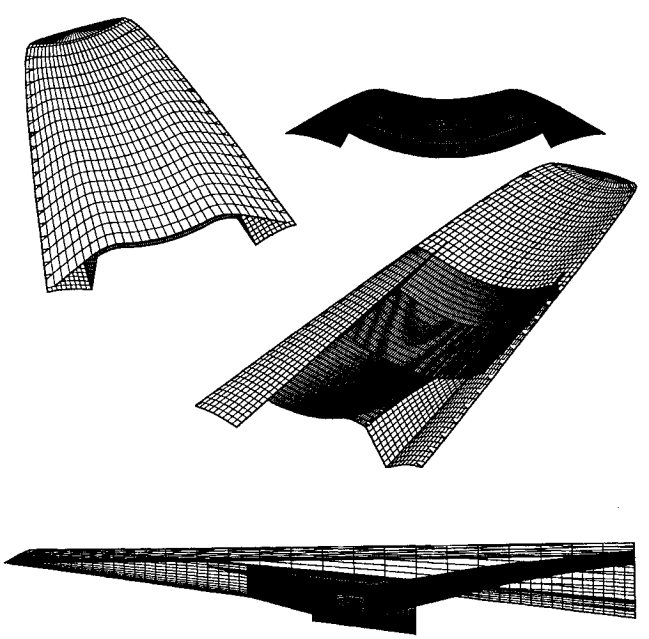

Fig. 15 Mach 14 baseline accelerator. β_{min} = 11 deg, p_{comb} = 50 kPa, T_{comb} = 1400 K.

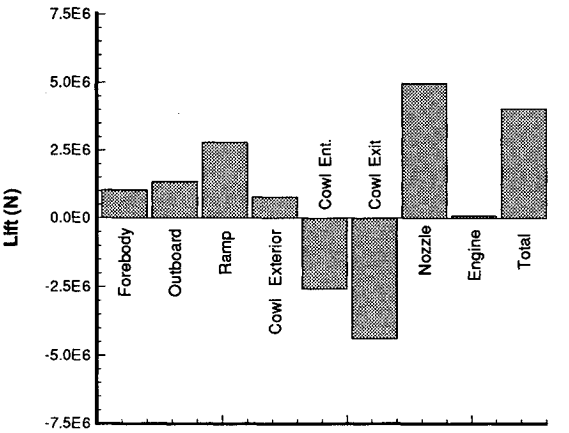

Fig. 16 Lift distribution on Mach 14 baseline accelerator. β_{min} = 11 deg, p_{comb} = 50 kPa, T_{comb} = 1400 K.

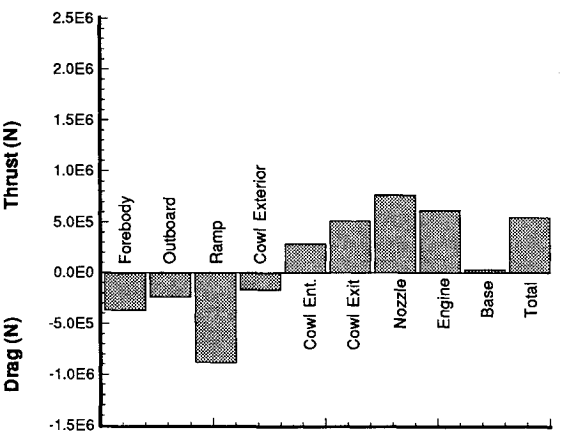

Fig. 17 Drag/thrust distribution on Mach 14 baseline accelerator. β_{min} = 11 deg, p_{comb} = 50 kPa, T_{comb} = 1400 K.

Figure 15 shows the resulting perspective and side views for the Mach 14 accelerator, which is similar to the Mach 10 accelerator configuration. Figures 16 and 17 show the lift and drag force distributions for the Mach 14 accelerator. Unlike the cruise vehicles, one of the primary surfaces for producing lift in an accelerator is the nozzle. Since the engine spans most of the vehicle, a large percentage of the downward momentum generated by the forebody is canceled by turning the flow into the engine. In addition the outboard sections of the undersurface are small. Thus, the cowl and nozzle must produce the remaining required lift to match the effective weight of the vehicle. The distribution of forces is similar for all three accelerators, except that the drag increases faster than thrust with increasing Mach number, resulting in a decreasing Isp_{eff}, as shown in Table 2.

Conclusions

Using the inverse design approach, the waverider and scramjet engine can be developed and optimized together to yield a vehicle with a high $Isp \times L/D$ for a cruise vehicle, or high Isp_{eff} for an accelerator. The ratios of L/W_{eff}, and T/D for cruise, in the objective functions are very effective. By the end of an optimization, these ratios are within a few percent, or less, of 1. The only exception to this occurs when the combustor entrance conditions are chosen such that the resulting flight altitude is out of the range where $L = W_{eff}$ is possible for an integrated configuration.

For the cruise configurations the total lift from the engine components, including the ramp, cowl and nozzle, is approximately zero. While there is almost no positive contribution to vehicle lift from the engine, the engine drag, particularly

from the ramp, is significant. Thus, the effect of an engine is to reduce the L/D of the cruise waverider. As Mach number increases, the engine size required increases, thus reducing further the L/D of the vehicle. An L/D of 4.70 and an Isp of 2786 s is achievable for a 60-m Mach 8 hydrogen-fueled cruise vehicle, flying at approximately 30.3 km. At Mach 10, at an altitude of 33.1 km, a 60-m cruise vehicle has an L/D of 3.48 and an Isp of 2417 s. Lower cruise Mach numbers would probably result in higher achievable L/D values while still maintaining $L = W_{\text{eff}}$. However, for maximum cruise at Mach 6 and below, ramjet engines would be preferable over scramjets.

To determine the configuration and L/D for the maximum L/D vehicle at a given Mach number, an optimization can be run without $(L/W_{\text{eff}})^a$ in the objective function. The resulting value of L/W_{eff} will indicate the flight altitude required to achieve this maximum value of L/D. This altitude may not be the desired cruise altitude, but it is beneficial to know the characteristics of the maximum L/D vehicle for a given Mach number to understand what the optimizer is doing when matching lift to effective weight. In general, whenever $(L/W_{\text{eff}})^a$ is removed from the objective function, β for the optimized configuration will be close to $\beta_{\min}$. Since volume decreases with decreasing β, the value of $\beta_{\min}$ should not be less than approximately 10 deg in the Mach number range considered to maintain reasonable vehicle volumes.

If the flight altitude is such that $L/W_{\text{eff}} < 1$ for the maximum L/D configuration, the optimizer will increase β to increase the vehicle lift and achieve $L = W_{\text{eff}}$. This results in a decrease in L/D, an increase in vehicle volume, and an increase in A_{cap}/S_p.

Inlet curves for cruise vehicles were allowed to become more elliptic compared to accelerators, since engine spans are smaller. The inlet curves for the Mach 8–10 cruise vehicles become more elliptic as Mach number increases. The Mach 8 curve is fairly circular, resulting in a flat nose and flat freestream upper surface. The Mach 10 curve is highly elliptic, resulting in a pointed nose and, as viewed from the base, a more pointed upper surface.

When the upper surface of a cruise vehicle is not expanded to reduce base area, the altitude at which the maximum L/D vehicle would fly to yield $L = W_{\text{eff}}$ is lower than that for an expanded configuration with the same generating shock angle β. This results due to a greater volumetric efficiency and a decrease in the lift component from the vehicle upper surface for an unexpanded configuration as compared to an expanded configuration.

The cowl lip was not forced to match the bow shock for a cruise vehicle since maximizing mass flow was not necessarily required. Several of the optimized cruise configurations result in cowl lips significantly inside the bow shock at the inlet station.

Optimizing with the accelerator objective function results in vehicles with longer nozzles and larger engine spans, as compared to cruise vehicles. Since most of the flow that passes over the forebody of the accelerator is turned into the engine, a large percentage of the forebody lift, depending on the cowl orientation, is canceled. Thus, to achieve $L = W_{\text{eff}}$, the nozzle of an accelerator, unlike a cruise vehicle, often contributes significantly to the vehicle lift. An Isp_{eff} of 1312 s, at an altitude of 31.8 km and a vehicle volume of 4135 m^3, results for a Mach 10 accelerator. Increasing the Mach number decreases the effective specific impulse achievable, primarily due to the large increase in drag with Mach number. At Mach 14 the Isp_{eff} is 531 s at an altitude of 36.9 km and a vehicle volume of 3902 m^3.

The requirements of maximizing engine mass flow, utilizing identical engine modules spanwise, and maintaining flowfield uniformity, result in accelerator configurations with highly circular inlet curves, to allow for large engine spans. The circular shaped inlet curves result in flat vehicle noses.

In contrast to the cruise vehicles, if more lift is required to achieve $L = W_{\text{eff}}$ for the accelerator configurations, β does not increase. For the accelerator configurations, β generally remains close to the value of $\beta_{\min}$. To increase vehicle lift, the engine of an accelerator moves forward along the length of the vehicle, increasing the nozzle lift.

Both cruise and accelerator vehicles should be designed to be trimmed at the on-design condition. Therefore, flap deflections that result in trim drag, are minimized, and L/D or Isp_{eff} are not severely reduced. The choice for the best configuration will therefore be highly influenced by the location of the c.p. relative to the c.g. of the vehicle.

The combined waverider and quasi-one-dimensional scramjet model lends itself readily to the development and optimization of the scramjet/waverider system, due to relatively short single iteration computation times. All of the computations were done on a Spark II computer. One optimization with 100 iterations takes an average of 400 s of cpu time to complete.

Future Work

Other waverider-generating flowfields such as elliptic cones or nonaxisymmetric bodies should be considered. In particular, for accelerator configurations, generating flowfields with a flat shock in the cross-sectional view at the engine inlet station are of interest.

Additional subroutines for other inlet types, other fuels such as hydrocarbons, and also boundary-layer effects, could be added to the current program. Another design variable that could be added in the optimization is the cowl orientation angle. Currently, the cowl surface is traced from the conical flowfield.

The current program uses a total vehicle density to determine the weight of the vehicle based on the volume. A more sophisticated model that takes into account surface area and engine size, e.g., would provide better estimates of vehicle weight. It would also be desirable to have information available for calculating the location of the c.g. for the vehicles throughout an optimization. This would allow a constraint on the relative locations of the c.p. and the c.g. to be implemented in the optimization.

The current study focuses on optimization at the on-design point for both the cruise and accelerator vehicles. If subroutines are added to calculate the off-design performance of the waverider forebody, and the inlet, combustor and nozzle, for flight from takeoff to the design-point, then optimization could be done along a trajectory for a given mission. The off-design performance of the nonaxisymmetric nozzle will substantially affect the pitching moment of the vehicle. The variation and location of the c.p. at off-design conditions could be included in the constraints.

Acknowledgments

The authors would like to acknowledge the Minta Martin Foundation at the University of Maryland and the Zonta International Foundation for financial support in the form of fellowships; Jeff Bowles and the NASA Ames Research Center for sponsoring a portion of this work, and Jeff Bowles for his assistance with vehicle weight.

References

[1]Bowcutt, K. G., "Hypersonic Aerodynamics: Basic and Applied," Hypersonic Short Course, Univ. of Maryland, College Park, MD, April 1991.

[2]O'Neill, M. K. L., and Lewis, M. J., "Scramjet Integration on a Waverider," First International Hypersonic Waverider Symposium, Univ. of Maryland, College Park, MD, Oct. 1990.

[3]Biasca, R. J., "Chemical Kinetics of Scramjet Propulsion," M.S. Thesis, Dept. of Aeronautics and Astronautics, Massachusetts Inst. of Technology, Cambridge, MA, Sept. 1988.

[4]Bowcutt, K. G., Anderson, J. D., and Capriotti, D., "The Viscous Optimize Hypersonic Waveriders," AIAA Paper 87-0272, 1987.

[5]Corda, S., and Anderson, J. D., Jr., "Viscous Optimized Waveriders Designed from Axisymmetric Flowfields," AIAA Paper 88-0369, 1988.

[6]Bauer, S., "Analysis of Two Viscous Optimized Waveriders,"

First International Hypersonic Waverider Symposium, Univ. of Maryland, College Park, MD, Oct. 1990.

[7]Takashima, N., and Lewis, M. J., "Navier-Stokes Computation of a Viscous Optimized Waverider," AIAA Paper 92-0305, 1992.

[8]Vanmol, D., "Heat Transfer Characteristics of Hypersonic Waveriders with Emphasis on the Leading Edge Effects," M.S. Thesis, Dept. of Aerospace Engineering, Univ. of Maryland, College Park, MD, 1991.

[9]O'Neill, M. K. L., and Lewis, M. J., "Optimized Scramjet Integration on a Waverider," AIAA Paper 91-1693, 1991.

[10]O'Neill, M. K., "Optimized Scramjet Engine Integration on a Waverider Airframe," Ph.D. Dissertation, Dept. of Aerospace Engineering, Univ. of Maryland, College Park, MD, 1992.

[11]McLaughlin, T. A., "Viscous Optimized Hypersonic Waveriders for Chemical Equilibrium Flow," M.S. Thesis, Dept. of Aerospace Engineering, Univ. of Maryland, College Park, MD, 1990.

[12]Small, W. J., Weidner, J. P., and Johnston, P. J., "Scramjet Nozzle Design and Analysis as Applied to a Highly Integrated Hypersonic Research Airplane," NASA TN D-8334, Nov. 1976.

[13]Shapiro, A. H., *The Dynamics and Thermodynamics of Compressible Fluid Flow*, Vol. 1, Wiley, New York, 1953, pp. 219–226.

[14]Rogers, R. C., and Schexnayder, C. J., Jr., "Chemical Kinetic Analysis of Hydrogen-Air Ignition and Reaction Times," NASA TP 1856, July 1981.

[15]Jachimowski, C. J., "An Analytical Study of the Hydrogen-Air Reaction Mechanism with Application to Scramjet Combustion," NASA TP-2791, 1988.

[16]Rogers, R. C., "Mixing of Hydrogen Injected from Multiple Injectors Normal to a Supersonic Airstream," NASA TN D-6476, Sept. 1971.

[17]Anderson, G. Y., and Gooderum, P. B., "Exploratory Tests of Two Strut Fuel Injectors for Supersonic Combustion," NASA TN D-7581, Feb. 1974.

[18]Drell, I. L., and Belles, F. E., "Survey of Hydrogen Combustion Properties," NACA Rept. 1383, 1957.

[19]Sobieczky, H., and Stroeve, J. C., "Generic Supersonic and Hypersonic Configurations," AIAA Paper 91-3301, 1991.

[20]Raymer, D. P., *Aircraft Design: A Conceptual Approach*, AIAA Education Series, AIAA, New York, 1989, pp. 155–158, 227–231.

[21]Ardema, M. D., Chambers, M. C., Terjesen, E. J., and Roberts, C. D., "Body Weight of Advanced Concept Hypersonic Aircraft," AIAA Paper 91-3180, 1991.

[22]Nelder, J. A., and Mead, R., "A Simplex Method for Function Minimization," *Computer Journal*, Vol. 7, Jan. 1965, pp. 308–313.